Applied Sciences, Computing and Energy, 2025, 3(1), 134-145

Tunable Electronic and Optical Properties of ZnO/Germanene Heterostructure for Solar Cells and Near Infrared Photodetector: A First-Principles Calculations

Asma'u Muhammad Hassan*, Abdullahi Lawal*, Aliyu Muhammed Aliyu, Ahmed Musa Kona, Dauda Abubakar, Sadiq Abubakar Dalhatu and Anas Manga
Received: 17 February 2025/Accepted: 18 June 2025/Published 01 July 2025

Abstract: *In this study, we investigated the electronic and optical properties of ZnO/germanene heterostructures using density functional theory (DFT) combined with the many-body G_0W_0 and Bethe–Salpeter equation (BSE) approaches. The quasiparticle band gaps of bulk and monolayer ZnO were calculated to be 3.20 eV and 3.79 eV, respectively, consistent with experimental values. For the ZnO/germanene heterostructure, the band gap decreased from 0.60 eV to 0.09 eV as the interlayer distance increased from 2.0 Å to 3.5 Å. The optical absorption spectra revealed strong absorption in the visible region, especially at an interlayer distance of 2.0 Å, where the optical gap was 0.6 eV. These results indicate that the ZnO/germanene heterostructure is a promising candidate for optoelectronic and solar cell applications due to its tunable band gap and efficient visible light absorption.*

Keywords*: DFT, G_0W_0, Germanen, Optical, Solar cell, Photodetector*

Asma'u Muhammad Hassan
Department of Physics, Faculty of Science, Sa'adu Zungur University, Gadau, Bauchi State, Nigeria
Email: asmaumh2000@gmail.com
Orcid id: https://orcid.org/ 0009-0002-7716-6204

Abdullahi Lawal
Department of Physics, Ahmadu Bello University Zaria, Kaduna State, Nigeria
Email: abdullahikubau@yahoo.com
Orcid id: https://orcid.org/0000-0003-1294-3180

Aliyu Muhammed Aliyu
Department of Physics, Faculty of Science, Sa'adu Zungur University, Gadau, Bauchi State, Nigeria
Email: aliyumaliyu@yahoo.com

Ahmed Musa Kona
Department of Physics, Federal University of Education Zaria, Kaduna State, Nigeria
Email: ahmedkona1979@gmail.com

Dauda Abubakar
Department of Physics, Faculty of Science, Sa'adu Zungur University, Gadau, Bauchi State, Nigeria
Email: dabubakar19@yahoo.com
Orcid id: https://orcid.org/0000-0002-3343-4943

Sadiq Abubakar Dalhatu
Federal University of Health Sciences Azare, Bauchi State, Nigeria
Email: sadgambaki@yahoo.com

Anas Manga
Department of Physics, Faculty of Science, Sa'adu Zungur University, Gadau, Bauchi State, Nigeria
Email: anasmanga002@gmail.com
Orcidid: https://orcid.org/0009-0007-4933-4895

1.0 Introduction

Since after isolating graphene from graphite, graphene-like two-dimensional (2D) materials have attracted a lot of attention because of their exciting mechanical, optical, and electronic properties (Novoselov et al., 2004). Particularly, germanene (Ge) is projected to have nanosheets that resemble graphene (Bechstedt et al., 2021). Germanene has a low-buckled structure that distinct it from graphene because of the coexistence of sp^2 and sp^3 hybridization (Xu et al., 2020). Remarkably, it has been discovered that germanene retain the Dirac-like electronic characteristics, and its hydrides exhibit characteristics that are comparable to those of graphene. Despite their great carrier mobility of $10^6\ cm^2V^{-1}s^{-1}$for graphene and $6\times 10^6\ cm^2V^{-1}s^{-1}$ for germanene (Ye et al., 2014), their metallic nature (zero-band gap) is the

limitation of utilizing them for transistor, optoelectronic, photodetector and nanoelectronics devices. Recently, there are several ways to modify the properties of 2D materials, creating heterostructures is one of them such as arsenene/graphene (Shang et al., 2020), germanene/antimonene (Ha et al., 2023), silicene/h-BN, germanene/germanene (Xu et al., 2020), arsenene/$FeCl_2$ (Song et al., 2016) and so on. Heterostructure is created by putting two-dimensional (2D) crystals on top of one another that have comparable atomic spacing and thermal expansion coefficients. More interestingly, the energy gap can be successfully moderated by adjusting the strain direction, and strength of the external electric field (E-field), as well as the interlayer spacing in the heterostructures. ZnO is a material that is widely used due to its superior mechanical and physical qualities. ZnO is typically an n-type material with a high resistivity due to a variety of defects, gaps, and vacancies; as a result, photodetectors based on it have modest response currents as well as poor responsivity. Various heterostructures based on ZnO have been reported, such as ZnO/MoS_2, the electronic and optical properties of ZnO/black phosphorus heterostructures have demonstrated that ZnO/germanene is a promising candidate for thermoelectric, solar cell and near infrared photodetector applications. The electronic and optical properties of C_2N/ZnO van der Waals heterogeneous were investigated by Song et al. in 2021 (Song et al., 2021). It is demonstrated that the unique photoelectric characteristics of the heterostructure interlayers, with photoelectron and holes situated on the C_2N and ZnO layers, respectively. As a result, the composite of the electron-hole pairs is decreased. The ZnO/alpha-CNH van der Walls (vdW) heterostructure was built by Yu et al. (Yu et al., 2019) in order to investigate the electronic and optical properties of ZnO/alpha-CNH heterostructure. The interface of g-ZnO/alpha-CNH heterojunction exhibits significant charge transfer, and there is improvement in the light absorption within visible light wavelengths. Since heterojunctions formed by other materials with germanene may change the physical and chemical properties of germanene, which in turn affects germanene performance in the device, research on germanene-based interfaces is crucial due to its high specific capacitance (Si et al., 2021) and high specific surface area (Xu et al., 2020). Therefore, combining application of ZnO and germanene would enhance the low absorbance of germanene. The heterojunction can efficiently detect both visible and ultraviolet light because it can effectively increase the range of visible light absorption to ultraviolet light. To reveal its hidden potential, a thorough understanding of the structural, electrical, and optical properties of ZnO/germanene is therefore necessary. In this study, highly accurate first principles approach was applied. We examined the material properties at the ground state using density functional theory (DFT). Although the DFT approach provides a precise depiction of material properties at ground states (Radzwan et al., 2017; Radzwan et al., 2020). This approach's drawback is its inability to provide accurate details regarding the material characteristics connected to the excited state because DFT Kohn-Sham energy cannot correctly prediction the quasiparticle (QP) band structure (Champagne et al., 2023). Therefore, bare DFT technique is not suitable for accurate electronic band gap prediction, especially for band gap semiconductor materials like ZnO (LAWAL, 2017; Radzwan et al., 2018). We constructed a novel 2D heterostructure of ZnO/germanene due to their structural similarity. GW approximation based on either self-consistent or non-self-consistent can be employed to address the aforementioned challenges (Yusuf et al., 2024). However, self-consistent GW is computationally expensive and impractical due to its complicated structure. A non-self-consistent GW approximation so-called one-shot GW approach (G_0W_0) is a preferable option in this regard. In this work, electronic and optical properties of ZnO/germanene heterostructure were computed using many-body perturbation theory (MBPT) within G_0W_0 approximation. Structural properties were investigated using bare DFT with various exchange-correlation functionals.

2.0 Computational Details

In this workIn, all calculations have been carried out using fully optimized lattice parameters and atomic internal coordinates using first-principles approach within density functional theory (DFT). All calculations were performed to determine the electronic and optical properties of ZnO/germanene heterostructures at varying interlayer distances. Ground-state properties were computed using Quantum ESPRESSO (Giannozzi et al., 2009). All structures were relaxed until forces on each atom were less than 0.01 eV/Å. The interactions between valence electrons and the ionic core potential of Ge, Zn, and O were modeled using norm-conserving pseudopotentials produced by the Rappe-Rabe-Kaxiras-Joannopoulos (RRKJ) technique (Bermeo-Campos et al., 2023; Giannozzi, 2010). Generalized gradient approximation (GGA) functional as parameterized by Perdew, Burke, and Ernzerhof (PBE) was used to treat the electron-electron for structural relaxation (Perdew et al., 1996). We used vdW-DF in addition to the semi-local GGA-PBE to account for the impact of van der Waals (vdW) interaction (Perdew & Zunger, 1981). For self-consistent computations, the convergence threshold energy was 10^{-9} eV, and all the lattice parameters were relaxed until the Hellmann-Feynman force acting on each ion is less than 5×10^{-5} eV/Å. For structural relaxation, the plane wave kinetic energy is 50 Ry, while the charge density is 475 Ry. Plane-wave kinetic energy cut-offs of 50 Ry and charge density of 350 Ry was found to be sufficient for calculating electronic band structures. The irreducible Brillouin zone was sampled with a set of 10×10×10 Monkhorst-Pack grid to generate k-points. For germanene/ZnO HTS band structure, the plane wave's kinetic energy cutoff is set at 340 eV with a grid of 10×10×1 k-points. To avoid unwanted interactions between the nearest slabs a large vacuum layer of 25 Å was used so that periodic images and the layer can be treated independently. A self-consistent convergence accuracy of $5 \times 10^{-6} eV$ per atom is chosen. The force between atoms has a convergence threshold of 0.01 eV, and its maximum displacement is 5×10^{-4} Å. Between germanene and ZnO, we adjust their distances to range from 1.5 to 3.5 Å, respectively. Quantum Espresso interface with YAMBO simulation package (Marini et al., 2009) for excited state calculations. On the other hand, to correct the underestimated band gap obtained within standard DFT calculations, Quantum Espresso interface with YAMBO simulation package (Marini et al., 2009) for calculating QP energies and optical properties. To perform one-shot GW calculation via YAMBO simulation package (Marini, 2016; Marini et al., 2009), the obtained results of KS energies and wave-functions from Quantum Espresso are used as input. The KS energies and wave-functions results are then used for constructing one-particle Green's function and static dielectric matrix. By employing plasmon-pole model, the static and dynamic dielectrics are constructed and the dynamic screening is obtained. The self-energy is then calculated as the product of one-particle Green's function (G) and screened Coulomb interaction (W) after using random phase approximation (RPA). Then quasiparticle (QP) equations are solved with self-energy (exchange and correlation part) replacing generalized gradient approximation potentials. The (QP) energies E_{nk}^{QP} correction to the Kohn-Sham eigenvalues E_{nk}^{DFT} is given in Equation (2) (Lawal et al., 2019).

$$\varphi_{nk}^{DFT} \mathrm{E}_{nk}^{DFT} = (\mathrm{T} + \mathrm{V}_H + \mathrm{V}_{ne} + \mathrm{V}_{XC}) \varphi_{nk}^{DFT} \quad (1)$$

$$\mathrm{E}_{nk}^{QP} = Z_{nk} \langle \varphi_{nk}^{DFT} | \Sigma_{GW}(\mathrm{E}_{nk}^{DFT}) - \mathrm{V}_{XC} | \varphi_{nk}^{DFT} \rangle + \mathrm{E}_{nk}^{DFT} \quad (2)$$

where T is the kinetic energy operator, V_{XC} is the DFT exchange-correlation potentials, V_{ne} is the potential of the nuclei, $\mathrm{V_H}$ is the Hartree potential, Σ_{GW} is the GW self-energy which is the product of one-particle Green's function, G and screened Coulomb potential, W as $i\mathrm{G_0W_0}$, and k and n are the k-point and band indices respectively, E_{nk}^{DFT} and φ_{nk}^{DFT} are the KS eigenfunctions and Z_n is the orbital renormalization factor which is defined as (Shishkin & Kresse, 2007).

$$Z_{nk} = \left[1 - \frac{\partial \langle \varphi_{nk}^{DFT} | \Sigma_{GW}(E_{nk}^{DFT}) | \varphi_{nk}^{DFT} \rangle}{\partial E_{nk}^{DFT}}\right]^{-1} \quad (3)$$

The k-points sampling in the Brillouin zone in one-shot GW calculations is 10×10×10 to ensure convergences of the QP energies because band gap value is very sensitive to k-point grid sampling. Since small energy cut-offs lead to false convergence of the QP band gap (Shahrokhi & Leonard, 2017), an energy cut-offs of 500 eV were found to be enough for reliable convergence. In this framework, the QP energies values have been converged with the number of unoccupied and occupied states more than 3000 bands.

3.0 Results and Discussion

3.1 Convergence Test of Ecut And K-Points

To obtain a well-converged total energy, all other parameters must be tested in relation to a convergence scale to guarantee that convergence is reached (Idris et al., 2020; Itas, Razali, et al., 2023). Thus, understanding convergences with regard to the mesh of k-points and the plane-wave kinetic energy cutoff is therefore crucial. Every plane-wave self-consisted field (PWSCF) total energy calculation starts with an analysis of convergences with regard to k-point sampling grid and plane-wave energy cutoff, since bad convergence always led to wrong total energy. According to Fig. 1(a), which presents the findings of the convergence test of ZnO, the total energy varies considerably with the kinetic energy cut-off until it reaches an energy cut-off where it becomes nearly stable. From 10Ry to 30Ry, the kinetic energy cut-off increases and stabilizes at 30Ry. It shows that there are no more increases in the kinetic energy cut-off from 30Ry, meaning that the total energy stays constant. Conversely, a well-converged energy cut-off is seen at 30Ry. For this reason, in both the bulk and monolayer ZnO situations, 50Ry was chosen as the plane wave basis set for the kinetic energy cut-off. Fig. 1(b), on the other hand, displays a well-converged result and illustrates how the total energy is independent of the number of k-points at a given place. There is a point at which the energy stays constant despite significant variations in the number of k-points. .

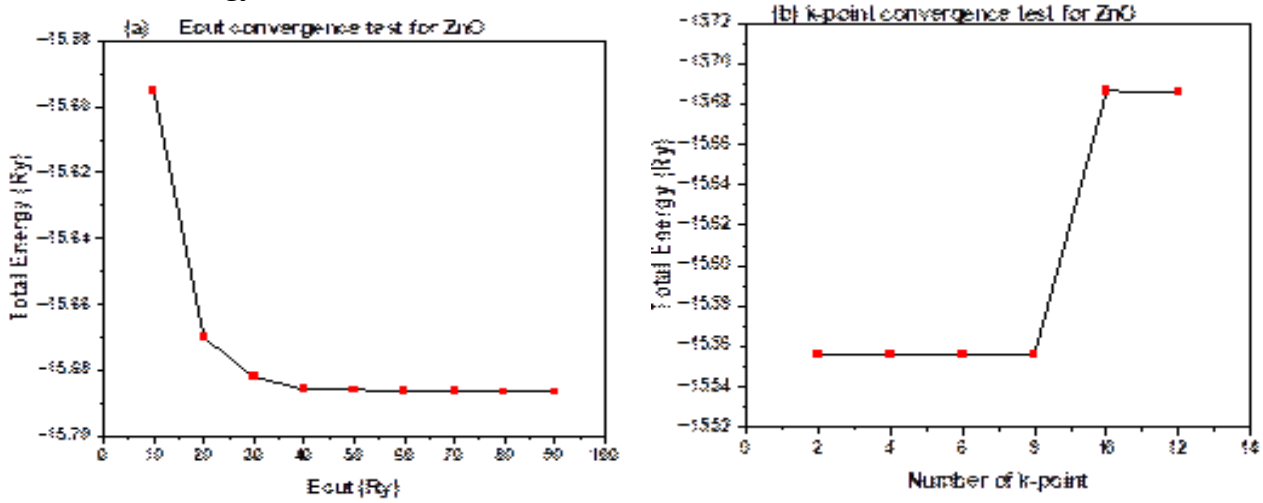

Fig. 1: (a) The convergence of total energy with respect to the kinetic energy cut-Off. (b) The convergence of the total energy with respect to the k-points grids

From 2×2×1 to 6×6×1 k-point grids, the total energy increases and reaches stability at 6×6×1. The Monkhorst and Pack approach can be used to select k-points in DFT calculations. The number of k-points to be employed in each direction in reciprocal space is one of the fundamental concepts of this method. 8× 8×1 k points were used in this study for all calculations

4.3 Structural Properties of ZnO in Bulk and Mono Layer Structure

The first stage in any first-principles calculation is geometrical relaxation, which helps to prevent a specific inaccuracy for precise predictions of other quantities such as electronic and optical properties (Yusuf & Lawal, 2025). Geometry optimization is a computational procedure that

involves adjusting cell parameters and atomic coordinates to decrease the structure's overall energy and produce a stable structure. Initially, the structural optimization procedure was carried out using the experimental lattice values. The ground state properties are found by fitting the computed total energy to Murnaghan's equation of state. Fig. 2 displays the geometric structures of bulk and monolayer ZnO. Table 1 illustrates how well the bulk structural parameters optimized under these conditions match their experimental values with little error.

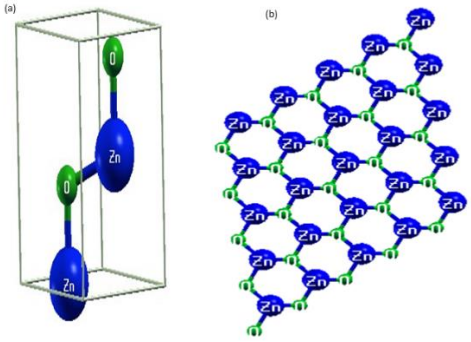

Fig. 2: Schematic diagram of Geometric Crystal of (a) Bulk ZnO (b) Monolayer ZnO

Table 1: Calculated and experimental lattice parameters for ZnO

Method	SOURCES	*a* (Å)	*c* (Å)
1	This work	3.2810	5.30682
2	(Tang et al., 2014)	3.2862	5.3005
3	(Karzel et al., 1996)	3.2501	5.2042
4	(Kisi & Elcombe, 1989)	3.2501	5.2071

3.2 Band structure of bulk and monolayer ZnO

To gain the insight into the electronic characteristics of Ge/ZnO at various interlayer distances, the band structures of Ge, ZnO in bulk and monolayer were computed. The results of electronic band gaps of germanene, monolayer ZnO and Ge/ZnO are shown along the high symmetry point Γ-M-K-Γ of the first Brillouin zone (BZ). The Fermi level is represented by the zero-energy scale on the band structure. Fig. 3(a) depicts the band structure of pure germanene with the Fermi level set to zero. Germanene is a material with a zero band-gap and Dirac cones at k points. The generalized gradient approximation (PBE-GGA) was selected in this work over the local density approximation (LDA) in DFT calculations because of its accuracy and reliability. Pure Ge exhibits zero band gap since the energy of the valence band maximum (VBM) and conduction band minimum (CBM) overlapped at the K point. The computed band gap for bulk ZnO was determined to be 0.89 and 2.5 eV for PBE and HSE, respectively. These values are in good agreement with previous first principles findings. However, because of the approximation utilized in the exchange correlation functional, the band gap values computed with PBE and HSE are smaller than the experimental finding of 3.15-3.4 eV. However, we have also carried out G_0W_0 corrections in order to address the discrepancy between the DFT calculation within GGA exchange-correlation potential and experimental data. We used MBPT within the G_0W_0 approximation to introduce self-energy corrections in the quasiparticle (QP) energy for an accurate band gap calculation. Applying G_0W_0 approximation, the energy gap of bulk ZnO was found to be 3.2 eV. It's interesting to note that the G_0W_0 approximation produces band gap value that match very well to experimental results. The predicted band gaps for PBE, HSE, and G0W0 in the case of monolayer ZnO were found to be 1.69, 2.8, and 3.79 eV, respectively, and these values are in good agreement with previous results.

3.3 Band structure of ZnO/germanene heterostructure

In general, combining materials with different topological ordering has generated a lot of

attention in order to find the new physical states for a range of applications that affect our day-to-day lives (Mondal & Pati, 2012). In order to assess the interaction and describe the necessary properties, theoretical methods is chosen in this study rather than experimental work because it is cheaper and less time consuming. ZnO may be interfaced with other materials, such as graphene, to create an interesting platform for investigating Dirac fermion events at interfaces. Strong light absorption in ZnO can be used to regulate the 2.3% optical absorption in germanene, while graphene offers a great transport channel for solar cell applications. Thus, combining germanene and ZnO can have some significant impacts without degrading the characteristics of either material. Additionally, a typical ZnO unit cell has a hexagonal crystal structure that resembles graphene. The unique properties of both germanene and ZnO motivate us to explore what will happen in ZnO/germanene by altering the distance between germanene and ZnO sheet. Fig. 5 and 6 show calculated band structure of germanene/ZnO by

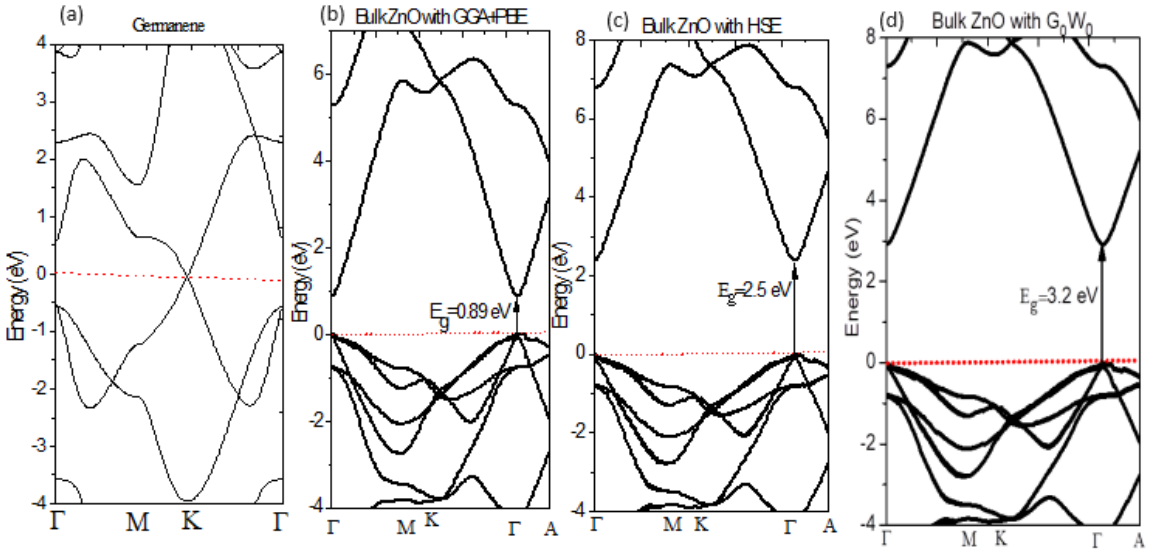

Fig. 3: Electronic band structure of (a) germanene (b) bulk ZnO with GGA+PBE (c) bulk ZnO with HSE (d) ZnO with G_0W_0

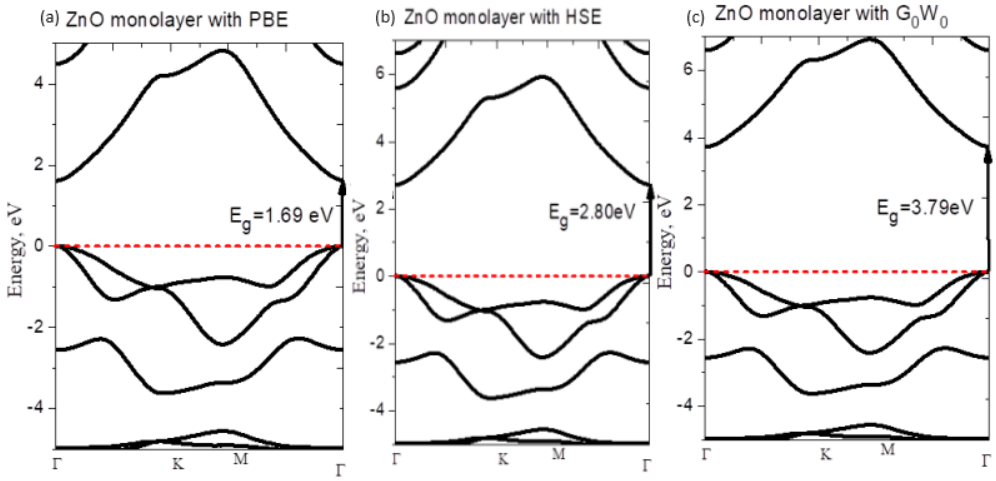

Fig. Error! No text of specified style in document.**: Electronic band structure of (a) monolayer ZnO with GGA+PBE (b) monolayer ZnO with HSE (c) monolayer with G_0W_0**

varying the interlayer distance from 2 to 3.5 Å respectively. It can be seen that with the increasing of the interlayer distance, the band gap increases from 0 eV at 2.0 Å to 0.6 eV and 0.38 eV at 2.5 Å and then decreases rapidly,

which may present a possible way to tune the band gap of germanene/ZnO indicating that at these distance germanene/ZnO can be used for solar cell application because the band gap value is within the visible light wavelengths. Fig. 6 shows that at d = 3.5 Å the interaction between germanene is a very weak which leads to almost closure of germanene Dirac states because the energy gap was just 0.09 eV. This indicates that the interfacing distance plays a vital role in providing the different strength of interlayer interactions between the adsorbate and the substrate surface; germanene and ZnO. These findings gave a tremendous impact since a noticeable energy gap of the germanene is created in the presence of ZnO sheet. This consequently leads the pathways of assembling a variety of applications with the semiconductor-like properties of germanene.

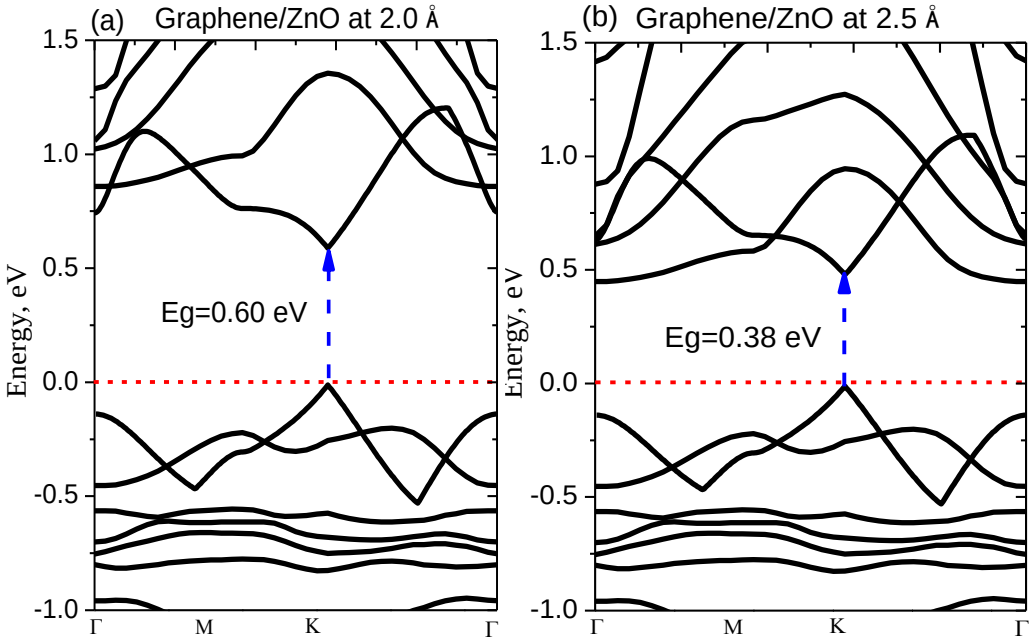

Fig. 5.: Band structures of germanene on top ZnO at (a) 2 Å (b) 2.5 Å interface

3.4 Optical Properties

The study of the optical properties of a material is crucial to get insight view about its characteristics for applications in the optoelectronic system and devices (Yusuf et al., 2025. From the comprehensive literature review, it is found that the exploration of the optical features relating to ZnO/germanene are scarcely done. To complete the study on optoelectronic properties, in addition to the electronic properties a comprehensive study is presented on the optical absorption of ZnO/ germanene by highly accurate method using random phase approximation (RPA) based on G_0W_0 (G_0W_0+RPA), which include electron-electron (e-e) interactions. Although optical properties calculation via G_0W_0+RPA is computationally expensive, it provides accurate description of the absorption spectra. Several studies have shown that inclusion of e-e interactions gives accurate description of the optical spectra (Escudero et al., 2017; Itas, Razali, et al., 2023; Itas, Suleiman, et al., 2023; Körbel et al., 2016; Rohlfing & Louie, 2000).

The optical parameters considered in this paper is imaginary part of dielectric function $\varepsilon_2(\omega)$ which correspond to the optical absorptions. The imaginary part $\varepsilon_2(\omega)$ of frequency dependent of the dielectric function relates to the manner by which light is absorbed by the medium (LAWAL, 2017; Lawal et al., 2017). The material's ability to absorb photon energy is described by its $\varepsilon_2(\omega)$. It is also well known that when light beams hit a material's surface, some of the energy is reflected back and some is

transmitted to the surface and the energy transfer to the surface is known as light absorption. From Fig. 7 (a, b and c); the calculated $\varepsilon_2(\omega)$ with show that the first critical point which sometimes called optical gap occur at 3.2, 3.79 and 0.6 eV for bulk, monolayer and ZnO/germanene at interlayer distance of 2.0 Å. These values are corresponded to QP band gap. In other words, the edge of optical absorption represents the inter-band transitions between the valence band maximum and conduction band minimum, which corresponds to the electronic band gap of the material under investigation. Optical gap of 0.6 eV and strong absorption within visible light waveleghts in ZnO/germanene suggest that the heterostruture consider in this work is a promising candidate for solar cells applications.

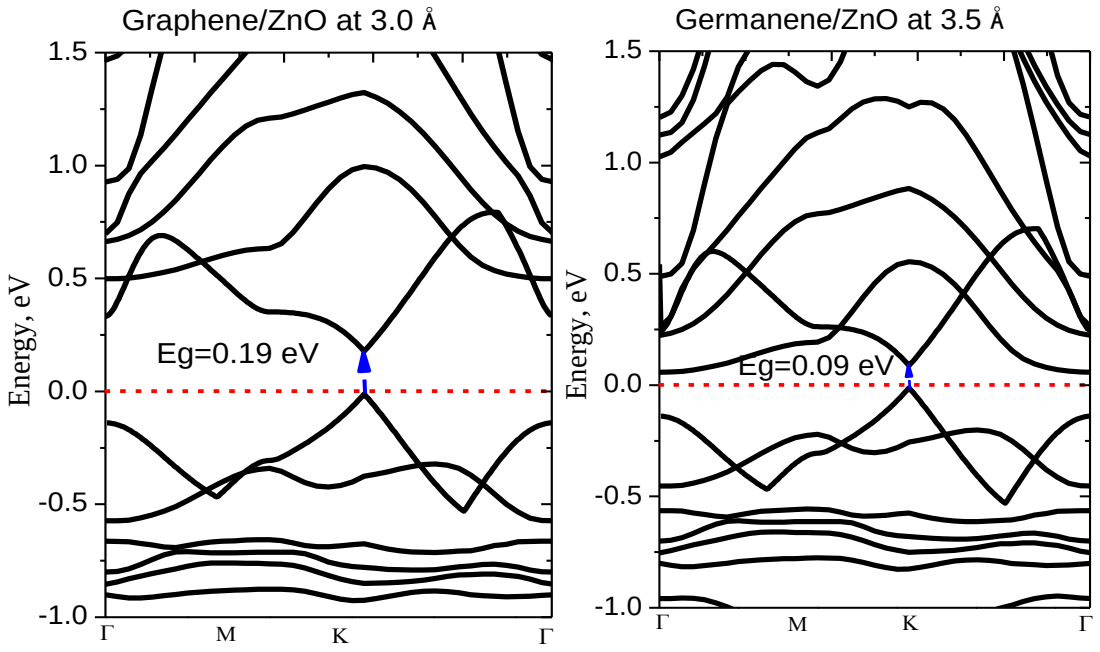

Fig. 6: Band structures of germanene on top ZnO at (a) 4 Å (b) 5 Å interface

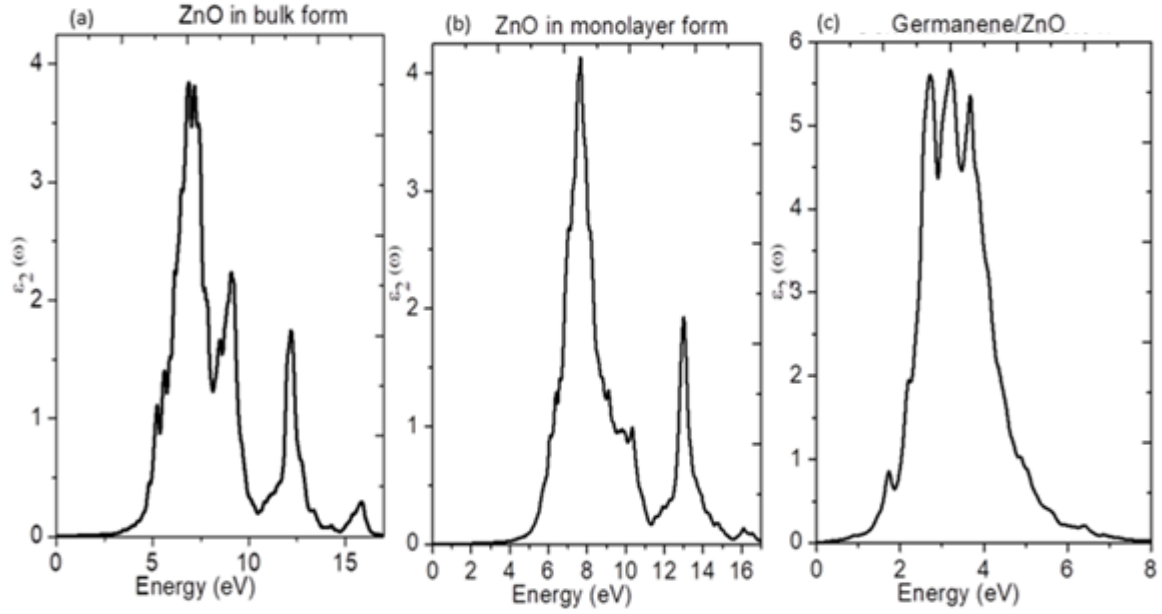

Fig. 8 : The imaginary part of frequeny-dependent dielectric functiron of: (a) bulk ZnO (b) monolayer ZnO (c) ZnO/germanene hetrostructure

4.0 Conclusion

In this paper, we conducted a comprehensive investigation of the electronic and optical properties of the ZnO/germanene heterostructure using a highly accurate many-body perturbation theory (G_0W_0) approach. The electronic properties were evaluated by varying the interlayer distance between 2.0 and 3.5 Å. The G_0W_0-calculated band gaps were 3.2 eV and 3.79 eV for bulk and monolayer ZnO, respectively. For the ZnO/germanene heterostructure, the band gap decreased from 0.6 eV to 0.09 eV as the interlayer distance increased from 2.0 Å to 3.5 Å, indicating strong interfacial coupling and tunability. The optical gap of the heterostructure at 2.0 Å was also 0.6 eV, aligning well with the corresponding quasiparticle band gap. Notably, the strong absorption of ZnO/germanene in the visible light region highlights its potential as an efficient candidate for solar cell applications. These findings contribute to the understanding of van der Waals heterostructures and open new avenues for their use in future optoelectronic devices.

5.0 References

Anton, L. (2009). *Improving the parallelisation and adding functionality to the quantum Monte Carlo code CASINO (Tech. Rep.).* HECToR: UK National Supercomputing Service.

Bechstedt, F., Gori, P., & Pulci, O. (2021). Beyond graphene: Clean, hydrogenated and halogenated silicene, germanene, stanene, and plumbene. Progress in Surface Science, 96(3), 100615. https://doi.org/10.1016/j.progsurf.2021.100615

Bermeo-Campos, R., Madrigal-Carrillo, K., Perez-Figueroa, S., Calvino, M., Trejo, A., Salazar, F., ... & Cruz-Irisson, M. (2023). Surface morphology effects on the mechanical and electronic properties of halogenated porous 3C-SiC: A DFT study. Applied Surface Science, 631, 157481. https://doi.org/10.1016/j.apsusc.2023.157481.

Champagne, A., Haber, J. B., Pokawanvit, S., Qiu, D. Y., Biswas, S., Atwater, H. A., ... & Neaton, J. B. (2023). Quasiparticle and optical properties of carrier-doped monolayer $MoTe_2$ from first principles. Nano Letters, 23(10), 4274–4281. https://doi.org/10.1021/acs.nanolett.3c00473.

Escudero, D., Duchemin, I., Blase, X., & Jacquemin, D. (2017). Modeling the photochrome–TiO_2 interface with Bethe–Salpeter and time-dependent density functional theory methods. The Journal of Physical Chemistry Letters, 8(5), 936–940. https://doi.org/10.1021/acs.jpclett.7b00066.

Ha, C. V., Thi, B. N. N., Trang, P. Q., Ponce-Pérez, R., Guerrero-Sanchez, J., & Hoat, D. (2023). Novel germanene–arsenene and germanene–antimonene lateral heterostructures: Interline-dependent electronic and magnetic properties. Physical Chemistry Chemical Physics, 25(20), 14502–14510. https://doi.org/10.1039/D3CP00590A.

Idris, M., Shaari, A., Razali, R., Lawal, A., & Ahams, S. (2020). DFT+U studies of structure and optoelectronic properties of Fe_2SiO_4 spinel. Computational Condensed Matter, 23, e00460. https://doi.org/10.1016/j.cocom.2020.e00460.

Itas, Y. S., Razali, R., Tata, S., Kolo, M., Lawal, A., Alrub, S. A., ... & Khandaker, M. U. (2023). DFT studies on the effects of C vacancy on the CO_2 capture mechanism of silicon carbide nanotubes photocatalyst ($Si_{12}C_{12-}X$; X = 1; 2). Silicon, 1–11. https://doi.org/10.1007/s12633-023-02518-4.

Itas, Y. S., Suleiman, A. B., Ndikilar, C. E., Lawal, A., Razali, R., Ullah, M. H., ... & Khandaker, M. U. (2023). DFT studies of the photocatalytic properties of MoS_2-doped boron nitride nanotubes for hydrogen production. ACS Omega. https://doi.org/10.1021/acsomega.3c02540.

Körbel, S., Kammerlander, D., Sarmiento-Pérez, R., Attaccalite, C., Marques, M. A., & Botti, S. (2016). Publisher's note: Optical

properties of Cu-chalcogenide photovoltaic absorbers from self-consistent GW and the Bethe-Salpeter equation [Phys. Rev. B 91, 075134 (2015)]. Physical Review B, 93(15), 159901. https://doi.org/10.1103/PhysRevB.93.159901.

Lawal, A. (2017). *Theoretical study of structural, electronic and optical properties of bismuth-selenide, bismuth-telluride and antimony-telluride/graphene heterostructure for broadband photodetector* . aster's thesis, Universiti Teknologi Malaysia.

Lawal, A., Shaari, A., Ahmed, R., & Jarkoni, N. (2017). First-principles many-body comparative study of Bi_2Se_3 crystal: A promising candidate for broadband photodetector. Physics Letters A, 381(35), 2993–2999. https://doi.org/10.1016/j.physleta.2017.07.020.

Lawal, A., Shaari, A., Ahmed, R., Taura, L., Madugu, L., & Idris, M. (2019). Sb_2Te_3/graphene heterostructure for broadband photodetector: A first-principles calculation at the level of Cooper's exchange functionals. Optik, 177, 83–92. https://doi.org/10.1016/j.ijleo.2018.09.102.

Marini, A. (2016). The Yambo code: *A comprehensive tool to perform ab-initio simulations of equilibrium and out-of-equilibrium properties*. APS Meeting Abstracts.

Marini, A., Hogan, C., Grüning, M., & Varsano, D. (2009). Yambo: An ab initio tool for excited state calculations. Computer Physics Communications, 180(8), 1392–1403. https://doi.org/10.1016/j.cpc.2009.02.003.

Mondal, W. R., & Pati, S. K. (2012). A study on the surface states of a topological insulator: Bi_2Se_3. arXiv Preprint, arXiv:1208.1482. https://arxiv.org/abs/1208.1482

Novoselov, K. S., Geim, A. K., Morozov, S. V., Jiang, D.-E., Zhang, Y., Dubonos, S. V., ... & Firsov, A. A. (2004). Electric field effect in atomically thin carbon films. Science, 306(5696), 666–669. https://doi.org/10.1126/science.1102896.

Perdew, J., & Zunger, A. (1981). Ab initio calculations of structural, elastic, and electronic properties of silver nitrides. Physical Review B, 23, 5048–5079. https://doi.org/10.1103/PhysRevB.23.5048.

Perdew, J. P., Burke, K., & Ernzerhof, M. (1996). Generalized gradient approximation made simple. Physical Review Letters, 77(18), 3865–3868. https://doi.org/10.1103/PhysRevLett.77.3865.

Radzwan, A., Ahmed, R., Shaari, A., Lawal, A., & Ng, Y. X. (2017). First-principles calculations of antimony sulphide Sb_2S_3. Malaysian Journal of Fundamental and Applied Sciences, 13(3), 285–289.

Radzwan, A., Ahmed, R., Shaari, A., Ng, Y. X., & Lawal, A. (2018). First-principles calculations of the stibnite at the level of modified Becke–Johnson exchange potential. Chinese Journal of Physics, 56(3), 1331–1344. https://doi.org/10.1016/j.cjph.2018.05.017.

Radzwan, A., Lawal, A., Shaari, A., Chiromawa, I. M., Ahams, S. T., & Ahmed, R. (2020). First-principles calculations of structural, electronic, and optical properties for Ni-doped Sb_2S_3. Computational Condensed Matter, 24, e00477. https://doi.org/10.1016/j.cocom.2020.e00477.

Rohlfing, M., & Louie, S. G. (2000). Electron-hole excitations and optical spectra from first principles. Physical Review B, 62(8), 4927–4944. https://doi.org/10.1103/PhysRevB.62.4927.

Shahrokhi, M., & Leonard, C. (2017). Tuning the band gap and optical spectra of silicon-doped graphene: Many-body effects and excitonic states. Journal of Alloys and Compounds, 693, 1185–1196. https://doi.org/10.1016/j.jallcom.2016.09.070.

Shang, Y., Wang, M., Hu, Q., Gao, Q., Xin, Y., Shi, H., ... & Huang, A. (2020). Permeability and mechanical properties of arsenene and arsenene/graphene heterostructure: First-principles calculation. Computational Condensed Matter, 23,

e00473. https://doi.org/10.1016/j.cocom.2020.e00473.

Shishkin, M., & Kresse, G. (2007). Self-consistent GW calculations for semiconductors and insulators. Physical Review B, 75(23), 235102. https://doi.org/10.1103/PhysRevB.75.235102.

Si, X., She, W., Xu, Q., Yang, G., Li, Z., Wang, S., & Luan, J. (2021). First-principles density functional theory study of modified germanene-based electrode materials. Materials, 15(1), 103. https://doi.org/10.3390/ma15010103.

Song, J., Zheng, H., Liu, M., Zhang, G., Ling, D., & Wei, D. (2021). A first-principles study on the electronic and optical properties of a type-II C_2N/g-ZnO van der Waals heterostructure. Physical Chemistry Chemical Physics, 23(6), 3963–3973. https://doi.org/10.1039/D0CP05884F.

Song, Y., Li, D., Mi, W., Wang, X., & Cheng, Y. (2016). Electric field effects on spin splitting of two-dimensional van der Waals arsenene/$FeCl_2$ heterostructures. The Journal of Physical Chemistry C, 120(10), 5613–5618. https://doi.org/10.1021/acs.jpcc.5b12141.

Xu, Q., Si, X., She, W., Yang, G., Fan, X., & Zheng, W. (2020). First-principles calculation of optimizing the performance of germanene-based supercapacitors by vacancies and metal atoms. The Journal of Physical Chemistry C, 124(23), 12346–12358. https://doi.org/10.1021/acs.jpcc.0c01818.

Ye, X.-S., Shao, Z.-G., Zhao, H., Yang, L., & Wang, C.-L. (2014). Intrinsic carrier mobility of germanene is larger than graphene's: First-principle calculations. RSC Advances, 4(41), 21216–21220. https://doi.org/10.1039/C4RA01785B.

Yu, Z.-L., Zhao, Y.-Q., Liu, B., & Cai, M.-Q. (2019). Breaking the anisotropy of α-CNH and improving the photoelectric performance by constructing van der Waals heterojunction. Applied Surface Science, 497, 143787. https://doi.org/10.1016/j.apsusc.2019.143787.

Yusuf, I. D., Suleiman, A. B., Lawal, A., Ndikilar, C. E., Taura, L., Gidado, A., & Chiromawa, I. M. (2024). Significant improvement in structural, electronic, optical and thermoelectric properties of $PdTe_2$ in bulk and monolayer phase: A G_0W_0 + BSE approach. Physica B: Condensed Matter, 685, 416015. https://doi.org/10.1016/j.physb.2024.416015

Yusuf, I., & Lawal, A. (2025). Structural, electronic and optical properties of PdSe2 in bulk and monolayer phases: A G0W0 calculation. Communication In Physical Sciences, 12(5), 1528-1537. https://dx.doi.org/10.4314/cps.v12i5.8

Yusuf, I. D., Suleiman, A. B., Lawal, A., & Ndikilar, C. (2025). G0W0+ BSE study of Optoelectronic and Thermoelectric Characteristics of Bulk and Monolayer PdS2 in Orthorhombic Structure for Solar Cell Applications. Physical Science International Journal, 29(4), 96-114. https://doi.org/10.9734/psij/2025/v29i4892

Declaration

Consent for publication

Not applicable

Availability of data

Data shall be made available on demand.

Competing interests

The authors declared no conflict of interest

Ethical Consideration

Not applicale

Funding

There is no source of external funding.

Authors' Contributions

Abdullahi Lawal led the study design, supervised the simulations, and co-wrote the manuscript. Asma'u Muhammad Hassan handled G_0W_0 and BSE calculations and contributed to methods development. Aliyu Muhammed Aliyu assisted with data analysis and literature review. Ahmed Musa Kona managed simulation optimization. Dauda Abubakar contributed to structural modeling, while Sadiq Abubakar Dalhatu and

Anas Manga supported interpretation and manuscript refinement,.